# Diagnostics of nanosecond dynamics of the plasma produced during KrF excimer laser ablation of zirconia in vacuum

Peng Li,[a] Daniel Lim, and Jyoti Mazumder[b]
*Center for Laser-Aided Intelligent Manufacturing, University of Michigan, Ann Arbor, Michigan 48109-2125*

(Received 6 February 2002; accepted for publication 11 April 2002)

A 248 nm KrF excimer laser was used to ablate the yttria stabilized $ZrO_2$ target in vacuum while an intensified charge coupled device camera was used to get the time-resolved side view images of the induced plume/plasma. Two components, plume and plasma, can be clearly distinguished from the images with delay time less than 300 ns. The center of the plasma is found moving along the direction tilted ~55°, instead of 90°, from the surface of the target while the processing laser came along ~40°. The movement velocities and the explosion rates of the plasma during the first 2 $\mu$s after the laser strike were calculated. Time- and spatial-resolved emission spectra from excited Zr atoms in the plasma have been measured to determine the corresponding excitation temperature. The dynamic evolution of the plasma is outlined based on the experimental results. © *2002 American Institute of Physics.* [DOI: 10.1063/1.1483394]

## I. INTRODUCTION

Yttria-stabilized zirconia (YSZ) films have attracted a lot of attention in research due to its specific optical, mechanical, thermal, and ionic conducting properties. The films can be used in applications such as optical and tribological coatings, thermal barrier, catalytic supports, as well as the substrate or buffer layer for the growth of high temperature superconductor $YBa_2Cu_3O_{7-x}$.

Pulsed laser ablation (PLA) deposition has been used widely to produce YSZ films since in pioneering work since 1987.[1,2] Although various processing parameters, such as laser wavelength and power, atmosphere and its pressure, substrate variety and temperature etc., have been explored to grow the films with desired properties, e.g., Refs. 3–17, and epitaxial YSZ films grown on Si[3,9,18] and InP substrates[17] have been reported, the influence of the processing parameters on the film quality is still under study.[19,20] As it has been pointed out, the plume/plasma produced during PLA may be critical for the growth of films with the required structure.[11,21] Understanding the properties of the plume/plasma, such as the component, velocity, density and temperature distribution in it, will be very helpful for control of the thin film growth. Time integrated and resolved optical imaging and spectroscopy and mass spectroscopy have been performed to get the information from PLA induced zirconia plume/plasma.[16,22–26] However, the detailed dynamic evolution of the plasma, especially during the first 2 $\mu$s after the laser strike, which contains abundant information on the interaction among laser, target and the initial plume, has not been sufficiently studied. And no temperature calculation from the spectroscopy measurements has been reported yet.

In this article, we present the experimental measurements on the optical imaging and emission spectroscopy, gathered by the intensified charge coupled device (ICCD) from the first 40 ns to 2 $\mu$s of the zirconia plasma/plume induced by PLA. The dynamic evolution of the plume/plasma and the excitation electronic temperature of the Zr atoms in the plasma have been discussed.

## II. EXPERIMENT

In our experiments, the hot pressed $ZrO_2$ target (PureTech Inc., stabilized with 5 wt. % $Y_2O_3$) was enclosed in a stainless-steel vacuum chamber, which was evacuated to less than $8\times10^{-7}$ Torr by a turbomolecular pump. The excimer laser (Lambda Physik, EMG 201) ran with KrF at $\lambda = 248$ nm with the pulse width at 20 ns. The repetition rate of the excimer was held to 2 Hz to avoid any possible interinfluence between the adjacent plume/plasma induced by the pulses. The angle between the laser beam and the surface of the target is ~40° and the incoming beam was focused to a 3 $mm^2$ area with its energy fluence at 1 $J/cm^2$. The target holder rotates and translates in the plane of its surface to continuously provide a fresh target surface to the ablating beam.

As depicted in Fig. 1, an ICCD (Princeton Instruments, $384\times576$ pixels with resolution of 23 $\mu$m) was put along the direction perpendicular to the laser beam to get the sideview image of the plume/plasma. The acquisition gate time on ICCD was set to 20 ns for delays less than 2 $\mu$s, while the delay time is defined as the time difference between the beginnings of the laser pulse and the gate. The gate was triggered by a photodiode monitoring the laser light at the exit of the excimer. Five acquisitions were accumulated for each measurement to improve signal to noise ratio and 2–4 measurements were averaged to get one image.

When the emission spectra were measured, the ICCD was mounted in the image plane of a ISA HR320 spectrometer fitted with a 2400 groove/mm grating. The spectrometer was oriented with the entrance slit parallel to the normal of the target surface and the image of the ablation point was

[a]Electronic mail: relax@umich.edu
[b]Author to whom correspondence should be addressed; electronic mail: mazumder@umich.edu

 

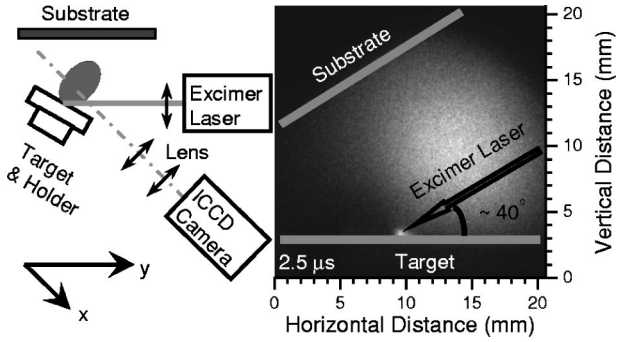


FIG. 1. Schematic of the experimental configuration and the ICCD image of the plasma. The image has been tilted as described in context.

positioned on the slit. The entrance slit width was set to 25 $\mu$m. The same trigger system as above had been used. Hundreds of to more than 10 000 pulses were gathered and averaged to obtain the spectra depending on the intensity of the emission at different delays.

An image of the plasma, gathered at a 2.5 $\mu$s delay with a gate of 100 ns, is also given in Fig. 1. As is shown, the images in this article have already been tilted to allow the direction along the target surface be horizontal for the convenience of analysis and description.

## III. RESULTS AND DISCUSSION

### A. Images of the plume and plasma

Figure 2 shows some images of visible emission (from 300 to 850 nm) at delays from 40 ns to 1.8 $\mu$s from the PLA induced YSZ plume/plasma in vacuum. Due to the fast decrease of the intensity versus delay, some images have been magnified in intensity to better show the shape and position variation of the plume/plasma. Same horizontal and vertical dimensions and configurations are used as the image in Fig. 1. It can be clearly seen that with the increase of the delay the whole part of the plume/plasma expanded and its center moved to the top-right direction. A circle in the 1.8 $\mu$s delay image indicates the point where the ablation laser hit the target. At the initial period, e.g., 40 and 50 ns delay, the plume/plasma remained just above this point and its expansion was normal to the target surface. The apparent horizontal shift of the center of the plasma can be seen starting from about 200–300 ns delay.

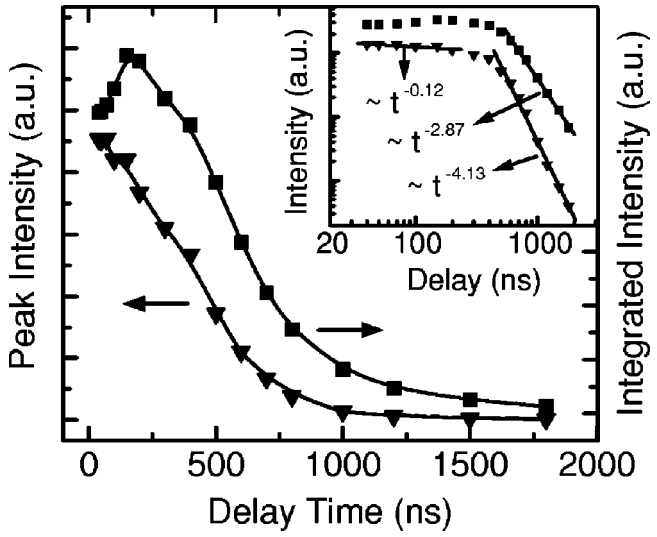


FIG. 3. The peak (triangles) and integrated (squares) intensity of the plume/plasma images vs delay time. Lines are guides for the eye. Inset: The log-log point and the power function fittings.

The decay of the peak and integrated intensities of the plume/plasma images in Fig. 2 are plotted in Fig. 3. More points on the delay are used than in Fig. 2. As illustrated in the log–log inset, the peak intensity of the emission decreases versus delay as the $t^{-0.12}$ law in the first ~200 ns and $t^{-4.13}$ after $t \sim 500$ ns. The integrated intensity also shows a faster decay, $t^{-2.87}$, when the delay is more than ~500 ns. The decrease in the intensity of the plasma is believed to correspond to the energy transferring from the excited electrons to the kinetic atoms.

Besides the evolution of the position, shape and intensity of the plume/plasma, the two components, a bright core and its blur ambient, in the images with small delays can be

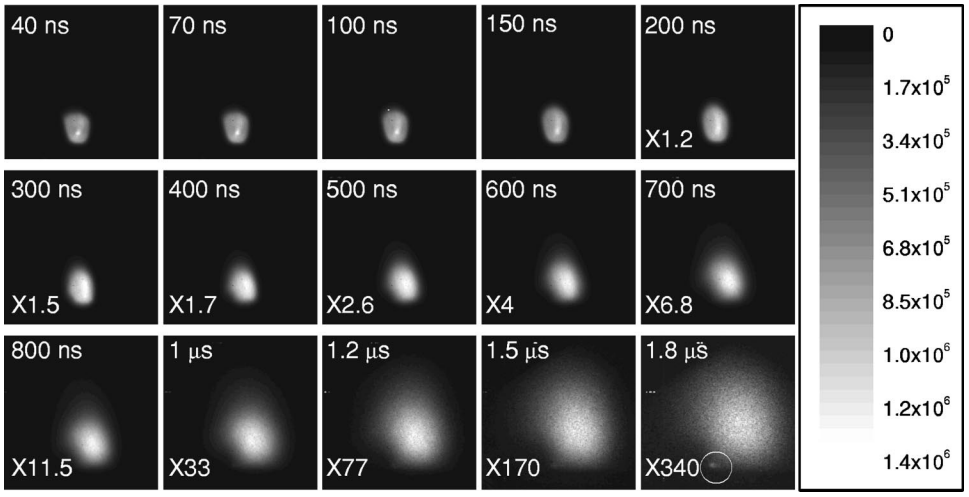


FIG. 2. ICCD images of the YSZ plume/plasma at the delays from 40 ns to 1.8 $\mu$s. Some images have been magnified in intensity according to the magnification marked at the left-bottom corner of the images. The images are all 20.6 mm×20.6 mm in actual size.

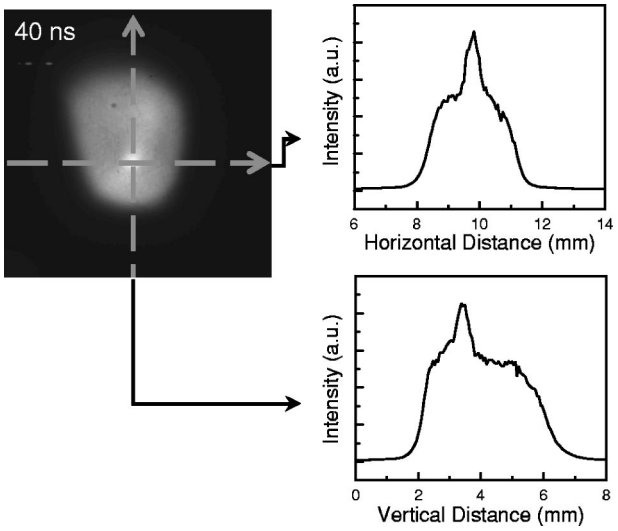


FIG. 4. Two-directions intensity analyses on the plume/plasma image.

clearly seen in Fig. 2. Figure 4 shows the intensity analyses along the horizontal and vertical directions across the center of the plume/plasma image at 40 ns delay. The variation of the intensity reveals two components in the image: one is the bright core, ~1 $mm^2$ in size and the other is the blur around it. In our emission spectra measurements, strong lines from $Zr^+$ were observed mainly in the area corresponding to the core part in the images while the ambient part only gave out some weak continuous emissions. This leads us to conclude that the core part is a kind of plasma, with atoms, ions and electrons in it, while the ambient part is more like a vaporous plume.

Because in most cases, there is no clear border for the plasma, an intensity isoline in the images needs to be defined to describe the size of the plasma. Based on the analyses of two components in the small delay images, it is found that the intensity value around 75% of the peak intensity in the image is about half the intensity of the corresponding plasma. Then, like the definition of full width at half maximum in spectra analysis, the area in the isoline with 75% of the maximum intensity in the image is used to characterize the size of the core plasma. After this definition, a center of the plasma is deduced by using the average of the pixels positions weighted with the corresponding intensity values at those positions in the image of the core plasma.

Figure 5 gives the positions of the centers and the outlines of the respective core plasma at different delays. For a better view, only five outlines are plotted in the figure to avoid too much overlap among them although a total of 16 different delays had been measured. The center of the plasma is found to move along a pretty straight line tilted ~55° from, instead of normal to, the target surface. The imaging measurements of the laser ablation of YSZ in oxygen, $10^{-3}$ and $10^{-5}$ Torr in our experiments, show similar results on the direction of the plasma movement. Although the oblique incidence of the laser is widely used in PLA of zirconia,[5,8,13,14,17,25,27,28] this non-normal movement of the plasma center has not been mentioned before. It is worth pointing out that the direction of the plasma movement

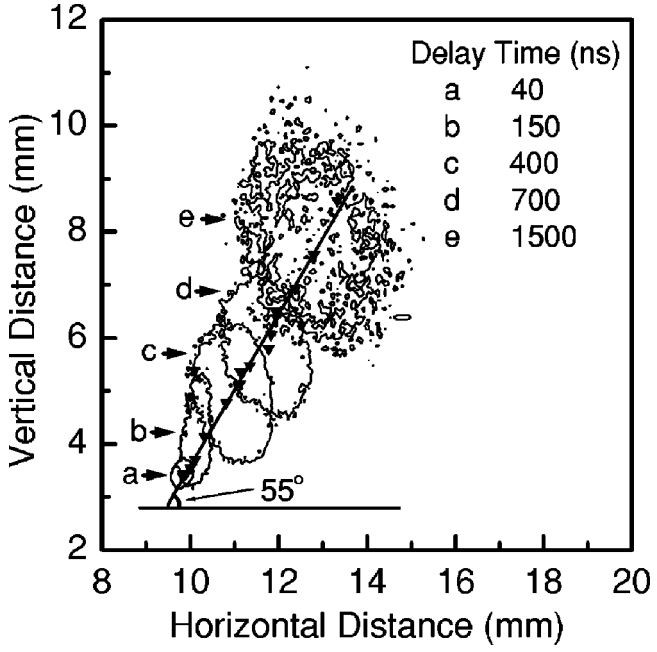


FIG. 5. The movement of the plasma centers and the evolution of the outlines.

should be well considered to produce high quality films.

Non-normal plume/plasma direction has been reported and discussed in other PLA systems before.[29–31] Pinto *et al.*[30] found the axis of the plume shifted slowly toward the direction of the laser beam with increasing exposure of the target to the laser beam during their ablating $YBa_2Cu_3O_{7-\delta}$ target and explained this by the formation of columnar structures on the modified target. Ito *et al.*[31] have mentioned a jet-like plasma growing toward incident laser beam during their laser ablation of aluminum by nanosecond Nd: yttrium–aluminum–gasses laser in air and explained it as the breakdown plasma of environment gas.

In our experiment, a YSZ target with a freshly polished surface was used to check the influence of the target surface on the direction of the plasma. It is found that the plasma direction tilted only ~5° from the normal of the target surface instead of the larger tilting angle for the target after cumulative laser pulse ablation. This result indicates that the

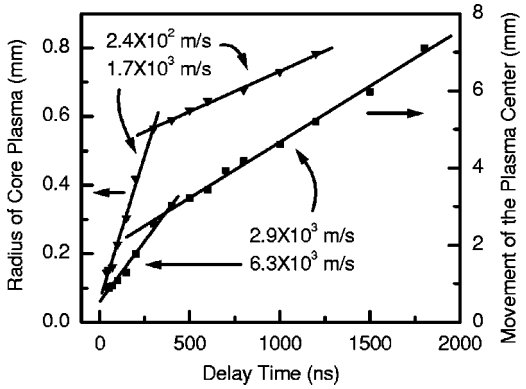


FIG. 6. The explosion of the core plasma in radius (triangle) and the movement of its center (square). Linear fittings of the corresponding data are also plotted.

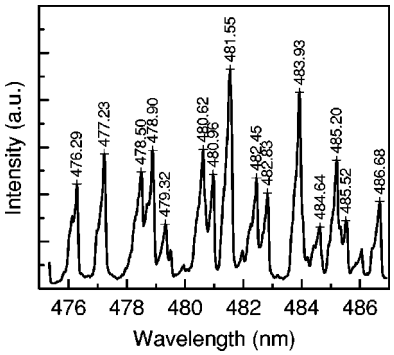


FIG. 7. A typical emission spectrum from ZrI for the 475–487 nm region.

morphology of the target surface contributes a lot to the determination of the plasma direction while further study is needed to understand the details.

Another possible contribution may come from the asymmetrical breakdown of the plume when plasma is produced. It is generally believed, i.e., in Ref. 27, that during the interaction of high-powered nanosecond excimer laser pulses with bulk targets, different regimes can be distinguished. After the beginning of the laser strike, the vapor/plume is produced from the target surface and expands. Then, the remaining part of the laser pulse will interact with the evaporated materials in the plume and the breakdown will start at the point where the power density of the laser beam reaches the threshold for the induced plasma.

In our experiment, the plume is found to expand quite perpendicularly to the target surface, from the images at small delays in Fig. 2. It is reasonable to assume that the breakdown will not happen at the exact center of the plume due to the inclining incident laser but at the part toward the laser. Because of the expansion of the plume itself, this part of the plume will give the subsequent plasma the initial velocity toward the incoming laser. Then the exact direction of the movement of the plasma center will be determined at last by this initial velocity and the interaction between the plasma and the target.

By the core plasma being treated roughly as round ones, their radii were calculated from the images. The increase of the radii versus time can be used to estimate the explosion rates of the plasma. As shown in Fig. 6, the explosion rate of the core plasma in the radius was about $1.7\times10^3$ m/s in the first ~300 ns and slowed down to $2.4\times10^2$ m/s after that. In the same figure, the velocity of the plasma center is also estimated from the distance among the centers at different delays. The center of the plasma moved in $6.3\times10^3$ m/s in the first 300–400 ns and decreased to $2.9\times10^3$ m/s thereafter.

### B. Excitation electronic temperature of the plasma

Partly because zirconium is a transition element which means it may have a rich energy level system, its emission spectrum contains abundant lines. Similar to previous articles,[22,26] strong emission from both Zr and $Zr^+$ have been observed in our experiment. Generally, $Zr^+$ lines locate below ~450 nm in the wavelength. To avoid the influence from the overlap between $Zr^+$ and Zr lines and to obtain enough lines and widely distributed upper energy levels needed in the temperature calculation, a region from 475 to 487 nm was carefully chosen to gather the emission spectra from Zr atoms. A typical spectrum obtained in our experiments is given in Fig. 7 and 15 Zr I lines have been identified by using the database in Refs. 32 and 33.

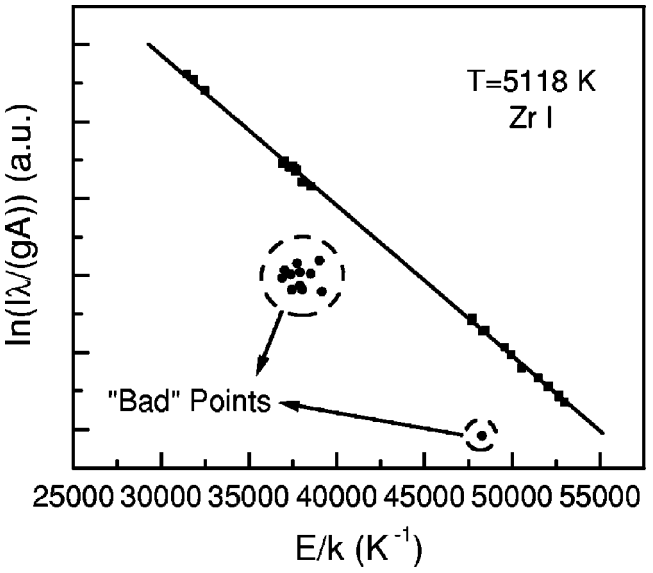


FIG. 8. Boltzmann plot for 39 lines in the 450–500 nm region.

The Boltzmann plot, $\ln[I\lambda/(gA)]$ versus $E/k$ is used to calculate the excitation electronic temperature of Zr atoms in the plasma, where $I$, $\lambda$, $g$, $A$, $E$, and $k$ are, respectively, the integrated line intensity over frequency, wavelength, upper level degeneracy, spontaneous emission coefficient, upper level energy, and Boltzmann's constant.[34] In our experiment, we found that not all the above 15 lines are good for the Boltzmann plot to calculate the electronic temperature. This was verified further by using the relative intensity data in Ref. 32, where the intensity data were determined from the measurement of arc emission and the existence of local thermal equilibrium was believed,[35] and the transition probabilities in Ref. 33. The Boltzmann plot for 39 lines listed in Ref. 32 from 450 to 500 nm is shown in Fig. 8. The data points can be clearly divided into two groups. Data in the first group can be well fitted with a straight line whose slope gave out the temperature 5118 K. Meanwhile, other points, in the dashed-line circle in Fig. 8, which we call ''bad'' points show a large deviation from the fitting line. The same phe-

TABLE I. The lines and relevant spectral data.

| Wavelength (nm) | Energy of upper level ($cm^{-1}$) | $g$ (degeneracy) | $A$ value ($10^7$/s) |
|---|---|---|---|
| 476.28 | 35 782 | 11 | 2.44 |
| 478.87 | 26 766 | 11 | 0.17 |
| 479.33 | 35 206 | 3 | 1.43 |
| 482.43 | 25 972 | 7 | 0.36 |
| 483.88 | 33 164 | 5 | 1.46 |
| 485.13 | 25 630 | 5 | 0.36 |
| 486.61 | 26 434 | 11 | 0.16 |

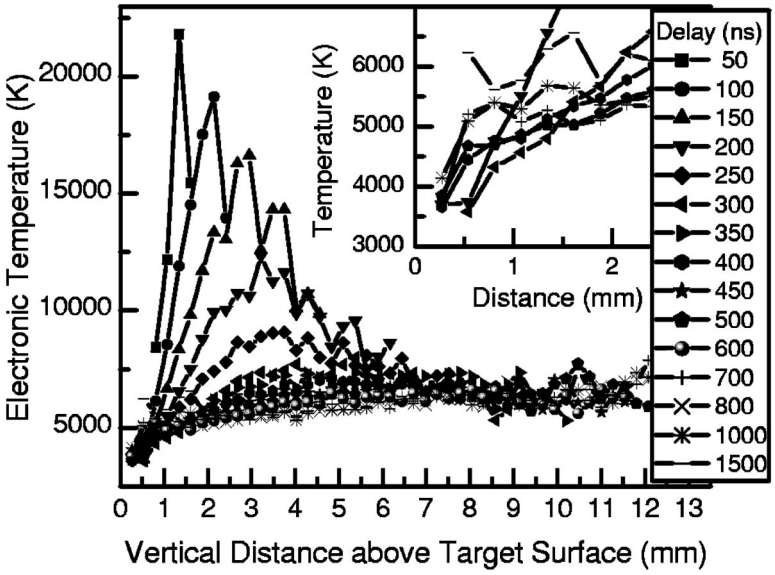


FIG. 9. The excitation electronic temperature of Zr I in the plasma. The inset gives a magnification of the near surface region. All the lines are just guides to eyes.

nomenon was observed in our data. It's not been known untill now whether the inaccuracy in the transition probabilities or the line itself is the reason for the behavior of the ''bad'' point.

After eliminating the bad lines, a total of seven lines have been finally chosen in our calculation of the temperature. The specifications of these lines from Kurucz's database[33] are listed in Table I. The result of the temperature calculation is displayed in Fig. 9. High electronic temperature, more than $2\times10^4$ K, had been reached in the core plasma, in the region from 1 to 1.5 mm above the target surface, at 50 ns delay after the laser strike. Then the temperature decreased, the high temperature core plasma expanded, and as the center moved against the surface of the target as well. This evolution shows good consistency with our results from the imaging measurements. However, the cooling rate of the plasma center is hard to determine from this figure because the plasma did not move along the direction normal to the target surface while the slit of the monochrometer was fixed at this direction. So the temperatures at large delays, e.g., more than 250 ns, plotted in Fig. 9 just represent the behavior of the plasma in the line normal to the target surface and going through the ablation point on the target. The temperature in this area decreased to about 6000 K after 300 ns delay and seemed to be stable out to the 1.5 $\mu$s delay, the limit in our experiment after which the emission signal is too weak to get a good signal. In our experiment, the front side of the core plasma had reached the substrate after 1 $\mu$s. This means that the plasma reached the substrate surface with its electronic temperature at ~6000 K

The inset in Fig. 9 shows the temperatures near the target surface. Not all lines in Fig. 9 are replotted here for a better view. It is seen, as the delay increases that the temperature went up from ~4500 to ~6000 K at a height of around 1 mm. This change is consistent with the appearance of the bright point in the images nearby the ablation point on the target surface at large delays; see the images at 1.2 and 1.5 $\mu$s in 2 and the one in Fig. 1. This phenomenon may be related to the thermal transfer around the ablation point in the target and between the target and the plasma nearby. Then, it is hoped that more information on the heating and cooling of the target during PLA can be obtained through the near surface imaging and spectra measurements.

## IV. SUMMARY AND CONCLUSIONS

In this study, we have used imaging and spectra measurements to probe the evolution of the plasma induced during PLA of the YSZ target in vacuum. Two components, plume and plasma, are identified at the early stage (delay less than 300 ns) of the plasma. The center of the plasma is found to move along the direction tilted ~55°, instead of 90° from the surface of the target while the processing laser came along at ~40°. The influence of the surface morphology of the target and the possible asymmetrical laser breakdown are discussed to explain this non-normal movement. It is pointed out that this kind of movement of the plasma should be considered in PLA deposition of high quality YSZ films. In the first 2 $\mu$s, the velocity of the plasma center decreased from $6.3\times10^3$ to $2.9\times10^3$ m/s. At the same time, the plasma exploded with the rate in radius from $1.7\times10^3$ to $2.4\times10^2$ m/s, while its intensity decreased very quickly.

The excitation electronic temperature of Zr atoms in the plasma has been figured out by analyzing the emission spectra. The core plasma is found to have an electronic temperature as high as $2\times10^4$ K at the 50 ns delay. The plasma front reached the substrate surface with its electronic temperature at ~6000 K. At the large delay region of more than 1 $\mu$s, the temperature increase of the plasma nearby the ablation point on the target has been observed. It is suggested to have a relation to the thermal transfer in the target and between the target and the plasma nearby.

In the future, the characterization of the films grown by PLA deposition will be connected to the plasma properties. A better control of the film quality is expected.

[1] H. Sankur, J. DeNatale, W. Gunning, and J. G. Neison, J. Vac. Sci. Technol. A **5**, 2869 (1987).

[2] P. T. Murray, J. D. Wolf, J. A. Mescher, J. T. Grant, and N. T. McDevitt, Mater. Lett. **5**, 250 (1987).
[3] D. K. Fork, D. B. Fenner, G. A. N. Connell, J. M. Phillips, and T. H. Geballe, Appl. Phys. Lett. **57**, 1137 (1990).
[4] P. Tiwari, S. M. Kanetkar, S. Sharan, and J. Narayan, Appl. Phys. Lett. **57**, 1578 (1990).
[5] S. B. Ogale, R. D. Vispute, and R. R. Rao, Appl. Phys. Lett. **57**, 1805 (1990).
[6] A. Kumar, L. Ganapathi, S. M. Kanetkar, and J. Narayan, Appl. Phys. Lett. **57**, 2594 (1990); J. Appl. Phys. **69**, 2410 (1991).
[7] M. C. Chuang and G. A. Smith, J. Vac. Sci. Technol. A **9**, 2397 (1991).
[8] F. Kokai, K. Amano, H. Ota, Y. Ochiai, and F. Umemura, J. Appl. Phys. **72**, 699 (1992).
[9] E. V. Pechen, R. Schoenberger, B. Brunner, S. Ritzinger, K. F. Renk, M. V. Sidorov, and S. R. Oktyabrsky, J. Appl. Phys. **74**, 3614 (1993).
[10] G. Reisse, B. Keiper, S. Weissmantel, H. Johansen, T. Martini, and R. Scholz, Phys. Status Solidi A **145**, 461 (1994).
[11] J. C. Delgado, F. Sánchez, R. Aguiar, Y. Maniette, C. Ferrater, and M. Varela, Appl. Phys. Lett. **68**, 1048 (1996).
[12] W. A. J. Quinton and F. Baudenbacher, Physica C **292**, 243 (1997).
[13] F. Hanus and L. D. Laude, Appl. Surf. Sci. **127–129**, 544 (1998).
[14] J. Gottmann and E. W. Kreutz, Surf. Coat. Technol. **116–119**, 1189 (1999).
[15] S. C. Moulzolf, R. J. Lad, and P. J. Blau, Thin Solid Films **347**, 220 (1999).
[16] C. Flamini, A. G. Guidoni, R. Teghil, and V. Marotta, Appl. Surf. Sci. **138–139**, 344 (1999).
[17] E. Vasco, L. Vazquez, M. Aguilo, and C. Zaldo, J. Cryst. Growth **209**, 883 (2000).
[18] C. H. Lei, G. V. Tehdeloo, M. Siegert, J. Schubert, and C. Buchal, J. Cryst. Growth **222**, 558 (2001).
[19] G. Reisse, S. Weissmantel, B. Keiper, B. Steiger, H. Johansen, T. Martini, and R. Scholz, Appl. Surf. Sci. **86**, 107 (1995).
[20] R. Aguiar, V. Trtik, F. Sánchez, C. Ferrater, and M. Varela, Thin Solid Films **304**, 225 (1997).
[21] A. A. Voevodin, J. G. Jones, and J. S. Zabinski, J. Appl. Phys. **88**, 1088 (2000) and references therein.
[22] D. P. Taylor, W. C. Simpson, K. Knutsen, M. A. Henderson, and T. M. Orlando, Appl. Surf. Sci. **127–129**, 101 (1998).
[23] A. Voss, J. Funken, M. Alunovic, Hsung, and E. W. Kreutz, Thin Solid Films **220**, 116 (1992).
[24] A. Voss, E. W. Kreutz, J. Funken, M. Alunovic, and H. Sung, Appl. Surf. Sci. **69**, 174 (1993).
[25] J. Göres, P.-J. Kung, D. B. Fenner, and J. I. Budnick, Rev. Sci. Instrum. **68**, 170 (1997).
[26] F. Sanchez, R. Aguiar, P. Serra, M. Varela, and J. L. Morenza, Thin Solid Films **317**, 108 (1998).
[27] R. K. Singh and J. Narayan, Phys. Rev. B **41**, 8843 (1990).
[28] G. Reiße, B. Keiper, S. Weißmantel, H. Johansen, R. Scholz, and T. Martini, Thin Solid Films **241**, 119 (1994).
[29] S. R. Foltyn, in *Pulsed Laser Deposition of Thin Films*, edited by D. B. Chrisey and G. K. Hubler (J Wiley, New York, 1994), p. 109.
[30] R. Pinto, S. P. Cai, C. P. D'Souza, L. C. Gupta, and R. Vijayaraghavan, Physica C **196**, 264 (1992).
[31] Y. Ito, I. Oguro, Y. Fukuzawa, and S. Nakamura, Proc. SPIE **4065**, 461 (2000).
[32] The National Institute of Standards and Technology (NIST), NIST Atomic Spectra Database, http://physics.nist.gov/PhysRefData/contents.html.
[33] P. L. Smith, C. Heise, J. R. Esmond, and R. L. Kurucz, Kurucz Atomic Line Database, http://cfa-www.harvard.edu/amdata/ampdata/amdata.html.
[34] A. Thorne, U. Litzén, and S. Johansson, *Spectrophysics: Principles and applications* (Springer, Heidelberg, 1999), p. 251.
[35] W. F. Meggers, C. H. Corliss, and B. F. Scribner, in *Tables of Spectral-Line Intensities Part I*, National Bureau of Standards Monograph 32 (U.S. GPO, Washington, D.C., 1961), p. III.